JSR Publications

Available Online

J. Sci. Res. **12** (3), 259-267 (2020)

JOURNAL OF SCIENTIFIC RESEARCH

www.banglajol.info/index.php/JSR

Study of the Structural, Magnetic and Transport properties of La^{3+} Doped Cu-Zn Ferrite

K. Nahar[1], M. A. Hossain[2], P. Roy[1*], M. N. I. Khan[3], S. S. Sikder[1]

[1]Department of Physics, Khulna University of Engineering & Technology, Khulna

[2]Department of Mechanical Engineering, City University of Hongkong, Hong Kong

[3]Materials Science Division, Bangladesh Atomic Energy Centre, Dhaka

Received 2 October 2019, accepted in final revised form 5 February 2020

Abstract

Crystalline La doped Cu-Zn ferrite with compositions $Cu_{0.15}Zn_{0.85}La_xFe_{2-x}O_4$ [x = 0.00, 0.02, 0.04, 0.06 and 0.08] were synthesized by using conventional solid state reaction method technique. X-ray diffraction pattern (XRD), scanning electron micrographs (SEM), hysteresis loop (M-H) curves and frequency dependent resistivity were employed to inspect the effect of La^{3+} doping on the structure, microstructure, magnetic and transport properties of the specimens. All the specimens exhibited fcc type cubic spinel structure where the particle size were within 500-1600 nm range. Magnetically ferromagnetic phenomenon was found for all the samples where the effect of La^{3+} doping consequence on the variation of various parameters like saturation magnetization (M_s), coercivity (H_c) and remanent magnetization (M_r). The resistivity tuned by frequency for all the samples presented the decreasing phenomenon with the increase of applied frequency.

Keywords: Ferrite; Solid state reaction; XRD; Hysteresis; Resistivity.

© 2020 JSR Publications. ISSN: 2070-0237 (Print); 2070-0245 (Online). All rights reserved.
doi: http://dx.doi.org/10.3329/jsr.v12i3.43406 J. Sci. Res. **12** (3), 259-267 (2020)

1. Introduction

There is an amplifying interest arises in ferrite materials due to their overwhelming applications in the field related to research and practical life. Their distinguished structural, electrical and magnetic properties are responsible for their wide applications. Structurally ferrites are sensitive materials and they exhibits high range of resistivity, low magnetic loss, high magnetic moments, chemical stability and mechanically hardness. These properties arises from the distributions of cations in tetrahedral A site and octahedral B site. All these can be highly influenced by various parameters like doping, variation of sintering temperature, purity of the reactants etc. [1,2].

Basically, rare earth materials exhibits some unique characteristics like large magnetocrystalline anisotropy, very large magnetostriction, large magnetic moments, large magnetocaloric effect etc. due to their localized nature of 4f electrons being totally

* *Corresponding author:* probal.phy@gmail.com

screened by 5s and 5p orbital [3]. The substitution of various divalent cations with any of the element in ferrite composition is remarkable one. In this regard, the doping of rare earth materials in ferrite compositions result a promising changes on the physical, electric and magnetic properties. Many works have been done on the substitutions of rare earth materials in ferrite [4-8].

Due to many supreme characteristics, the rare earth substituted spinel ferrites have drawn attention extensively in modern technologies. They have vast applications in the field of ferrofluid technologies, advanced microelectronics, microwave absorbing materials, high frequency data storage etc. Moreover, high frequency accessible networks and internet accessible smartphones are flawless examples of the applications of such type of materials [9,10].

The microstructure and the characteristics of these ferrite materials are sensitive enough due to the preparation methodology. There are many methods of sample preparation like solid state reaction method, chemical co-precipitation method, spray pyrolysis, sol-gel synthesis, hydrothermal synthesis etc. The physical and chemical properties of the samples may vary due to the variation of synthesis techniques.

Our previous work was based on the structure and frequency dependent permeability, dielectric and temperature dependent resistivity study of $Cu_{0.15}Zn_{0.85}La_xFe_{2-x}O_4$ ferrite [9]. The present work is the extension of our previous work and the purpose of our present investigation is to observe the synthesis of $Cu_{0.15}Zn_{0.85}La_xFe_{2-x}O_4$ materials by solid state reaction method and hence to inspect the effect of Lanthanum (La) doping on the structural properties including elaborate XRD study and surface morphology, magnetic properties and frequency dependent resistivity of Cu-Zn ferrite.

2. Experimental

The powdered composition of $Cu_{0.15}Zn_{0.85}La_xFe_{2-x}O_4$ [x = 0.00, 0.02, 0.04, 0.06 and 0.08] were synthesized by conventional solid state reaction method where analytical grade of CuO, ZnO, La_2O_3 and Fe_2O_3 were used as reactant where all the elements have purity~ 98%. Firstly all these powdered reactants were taken for grinding operation for 6 hr at room temperature so that reaction can take place. In order to get crystalline phase, all the samples were taken for calcination at 800 °C for 3 h. Then all the pre-sintered samples were taken for grinding again for 3 h and then pellet shape was made using hydraulic press using uniaxial pressure of 15 MPa where each pellet contains 0.5 mg of samples. All the samples were sintered at 1150 °C for 6 h. Finally found sintered pellets were taken for various characterizations.

The structural properties were observed by X-ray diffraction pattern for both as-dried and La doped samples. The X-ray powder diffraction was done by Cu-K_α (λ = 1.54 Å) radiation. The morphological properties were inspected by Scanning Electron Microscope. To study magnetic properties, hysteresis loops were taken for all the samples by Vibrating Sample Magnetometer (VSM) of model Microsence EV7. Finally the transport properties were observed from some data that were taken by Impedance Analyzer.

3. Results and Discussion

The structural properties, phase and site occupancy are investigated form the X-ray diffraction pattern for $Cu_{0.15}Zn_{0.85}La_xFe_{2-x}O_4$ for both as-dried samples and La doped samples that are shown in Fig. 1(a). All the samples show expected crystallization along with well-defined diffraction lines. The XRD patterns were indexed with the plane of (111), (220), (311), (222), (400), (422), (333) and (440) which are either even or odd confirms the evolution of single phase fcc type spinel structure [11,12]. The small secondary peak of $LaFeO_3$ are found for the samples with La doping from x= 0.04-0.08 that are denoted as * in Fig. 1(a). These small secondary peaks are found may be due to the preparation of the samples using raw CuO, ZnO and La_2O_3 [13,14].

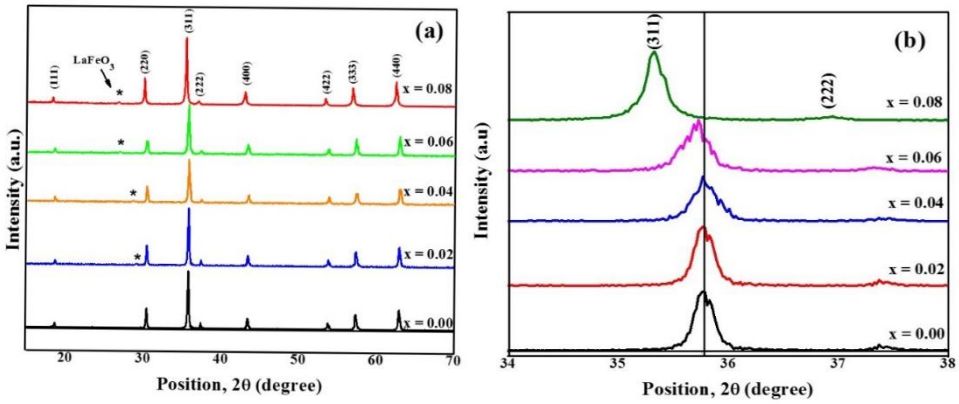

Fig. 1. (a) XRD pattern of $Cu_{0.15}Zn_{0.85}La_xFe_{2-x}O_4$; (b) Shifting of XRD plane for (311).

Fig. 1(b) presents the trend of the shifting of XRD pattern with the increase of La content. Basically this shifting occurs due to the change in chemical composition or due to strain as well as d-spacing i.e., lattice parameter which was determined by the use of Nelson- Relay function (N-R function) denoted as F(θ), where

$$F(\theta) = \frac{1}{2}\left(\frac{\cos^2\theta}{\sin\theta} + \frac{\cos^2\theta}{\theta}\right) \quad (1)$$

The variation of lattice parameter is shown in Fig. 2(a). Here, peaks shifted towards the left direction and the lattice parameter changed randomly but shows increasing phenomenon with the increase of La content. The ionic radius of doping element La^{3+} is 0.1172 nm that is greater than the Fe^{3+} (0.069 nm) which is responsible for the left shifting of the XRD pattern [15]. Fig. 2(b) delineate the variation of bulk density (d_B)and X-ray density (d_x) with respect to the increase in La content. The bulk density was measured by following the usual mass and dimensional consideration whereas the molecular weight and the volume of each sample provided the quantity of X-ray density. The following equations were used for measuring those parameters [16].

$$d_B = \frac{m}{V} = \frac{m}{\pi r^2 h} \quad (2)$$

and

$$d_x = \frac{8M}{na^3} \quad gm/cm^3 \quad (3)$$

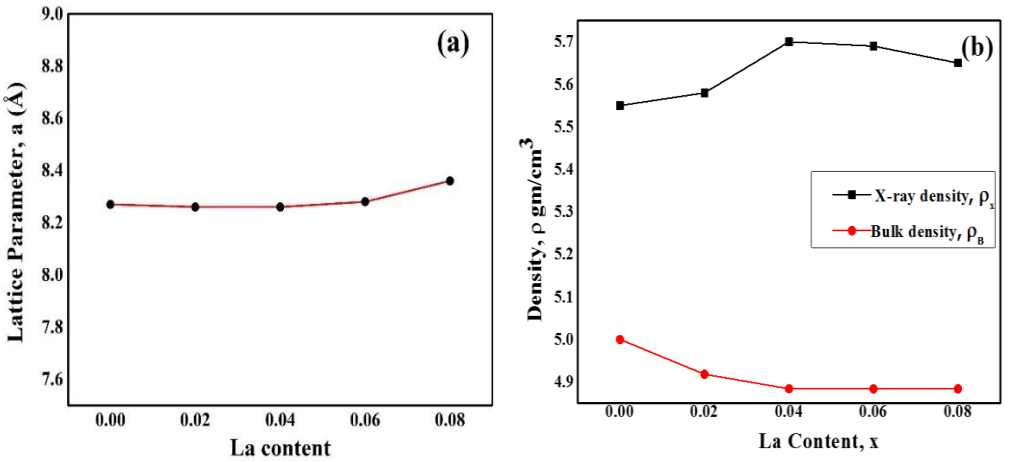

Fig. 2. Variation of (a) lattice parameter and (b) X-ray density and bulk density of $Cu_{0.15}Zn_{0.85}La_xFe_{2-x}O_4$ as a function of La content.

The X-ray density increases initially and then decreases which may be due to the presence of pores during the time of synthesis. This increase of X-ray density may be due to the increasing phenomenon of lattice parameter as well as left shifting of XRD peaks. The porosity also exhibits the changing phenomenon as like as the variation of X-ray density. The bulk density exhibits the decreasing phenomenon initially and then remains constant from a point with the increase of La substitution. The decreasing phenomenon of bulk density happens on account of the increasing intergranular porosity which is the result of discontinuous grain growth [17].

Table 1. Average grain size from SEM and porosity (from XRD) of La doped Cu-Zn ferrite.

Name of the sample	Contents	Avg. grain size (nm)	Porosity (%)
$Cu_{0.15}Zn_{0.85}Fe_2O_4$	x = 0.00	1600	9.92
$Cu_{0.15}Zn_{0.85}La_{0.02}Fe_{1.98}O_4$	x = 0.02	1230	11.87
$Cu_{0.15}Zn_{0.85}La_{0.04}Fe_{1.96}O_4$	x = 0.04	860	14.33
$Cu_{0.15}Zn_{0.85}La_{0.06}Fe_{1.94}O_4$	x = 0.06	650	14.18
$Cu_{0.15}Zn_{0.85}La_{0.08}Fe_{1.92}O_4$	x = 0.08	580	13.58

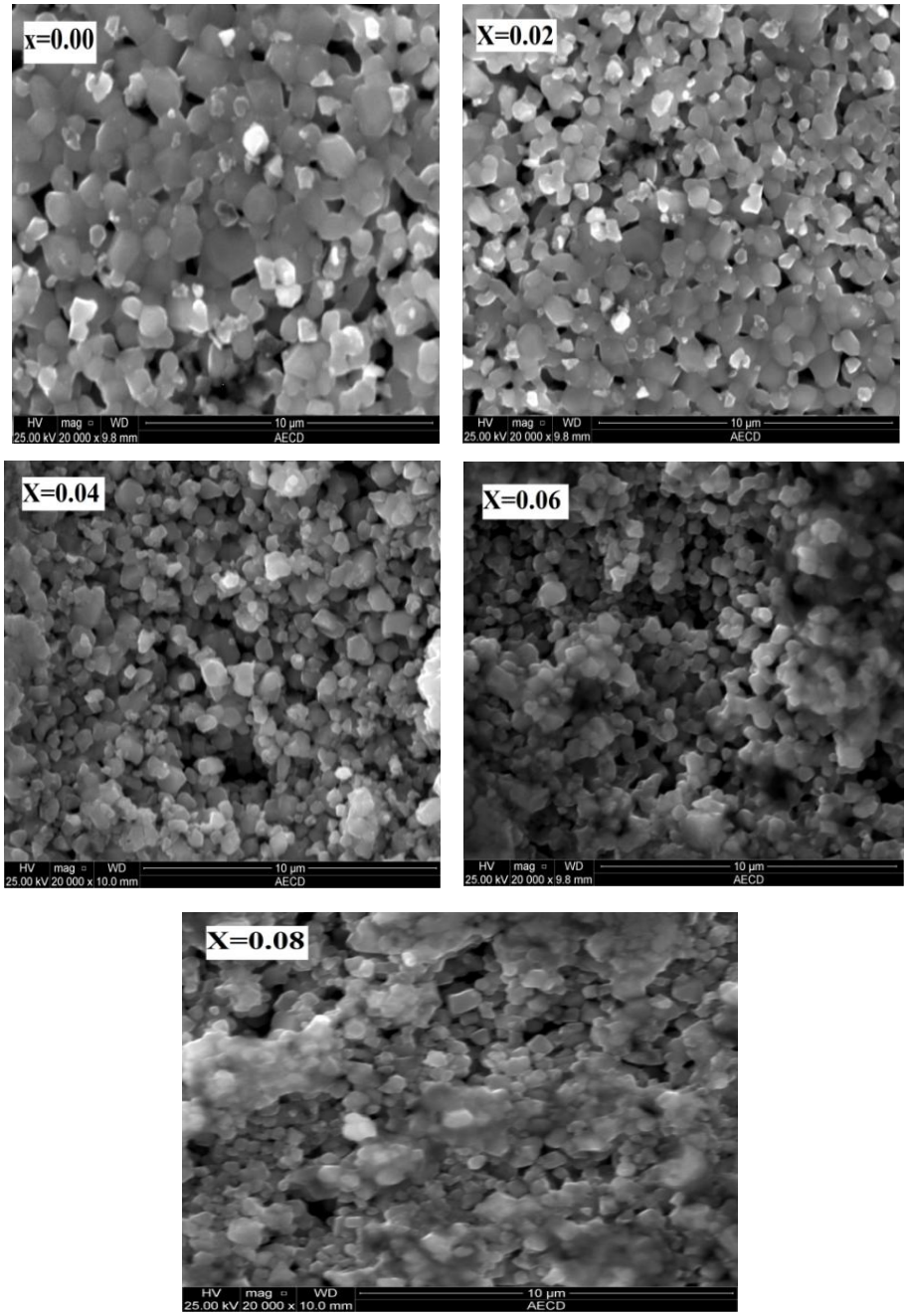

Fig. 3. SEM micrographs of $Cu_{0.15}Zn_{0.85}La_xFe_{2-x}O_4$, [x = 0.00, 0.02, 0.04, 0.06 and 0.08].

Fig. 3 shows the SEM micrographs of both as-dried and La doped samples. The SEM micrographs delineate the formation of microstructures having irregular grain size. The

microstructure consists of a bigger matrix of ferrite grain and also a smaller matrix of $LaFeO_3$ secondary phase at the grain boundary that was also confirmed in XRD. Intergranular pores are also noticeable for all the compositions. For each samples, several micrographs were taken to estimate the average grain size. The variation of grain size with respect to the concentration of La is presented in Table 1. The addition of La consequences a significant change in grain size. Without La^{3+} doping the Cu-Zn ferrite shows clear grain boundaries with very small grain boundary phase. With the addition of La^{3+}, the grain size decreases and the matrix of $LaFeO_3$ grain boundary phase increases. This decrease in the grain size can be responsible for some reasons that are mentioned as follows. Because of the larger bond energy of La^{3+}- O^{2-} in comparison with Fe^{3+}- O^{2-}, it is required higher energy for La^{3+} to enter into the lattices to form La^{3+}- O^{2-} bond. It causes higher thermal stability of La doped Cu-Zn ferrite rather than the undoped Cu-Zn ferrite, therefore it is required more energy to form crystallization due to doping [18,19]. Moreover, the pinning of $LaFeO_3$ at the grain boundary also obstacles the growth of crystallization [18].

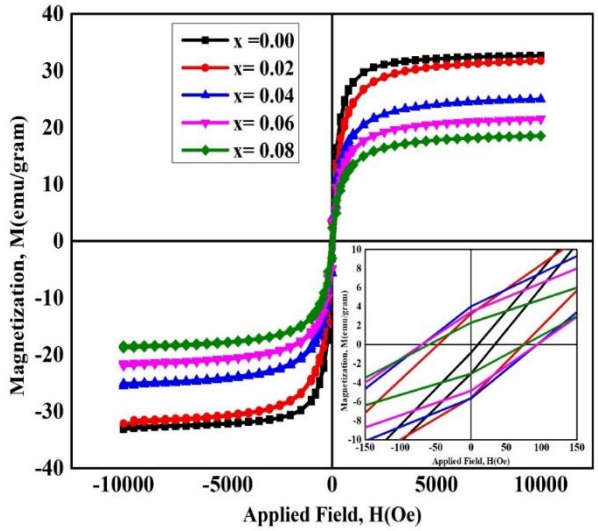

Fig. 4. Hysteresis loops (M-H curve) of $Cu_{0.15}Zn_{0.85}La_xFe_{2-x}O_4$, [x = 0.00, 0.02, 0.04, 0.06 and 0.08].

Table 2. Saturation magnetization (M_s), coercivity (H_c), remanent magnetization (M_r) and remanent ratio of La doped Cu-Zn ferrite.

Content	M_s (emu/gm)	H_c (Oe)	M_r (emu/gm)	M_r/M_s
x= 0.00	32.5	10	0.8	0.025
x= 0.02	31.6	60	3.2	0.1
x= 0.04	24.9	81	3.8	0.153
x= 0.06	21.3	80	3.3	0.155
x= 0.08	18.4	67	2.2	0.119

To investigate various magnetic properties, the hysteresis loops are taken for both as-dried samples and the La doped samples with maximum applied field of 10 kOe. Fig. 4

expresses the combined hysteresis graphs for all the samples. The magnitude of various magnetic parameters like saturation magnetization (M_s), remanent magnetization (M_r), remanent ratio (M_r/ M_s) and coercivity (H_c) are shown in Table 2. The M-H graphs of all the samples show the ferromagnetic behavior. The variation of La content exhibits remarkable changes on all these parameters. It is noticeable here that with the increase of La^{3+} content on Cu-Zn ferrite, saturation magnetization (M_s) and remanent magnetization (M_r) decreases. However, the coercivity (H_c) increases with the increase in La^{3+} content. Distribution of Fe^{3+} in various sites, magnetocrystalline anisotropy, Grain size, crystal defects, imperfection in lattice, porosity etc affects these magnetic parameters directly or indirectly [20-22]. Moreover, the double exchange Fe^{3+}-Fe^{2+} interactions are also attributing on the ferromagnetic ordering of all the materials [23].

The variation of electrical resistivity as a function of frequency are shown in Fig. 5 for both undoped and La doped Cu-Zn ferrites. The variation of electrical resistivity with respect to the frequency can be expressed as the following relation [24],

$$\rho = \frac{1}{\omega \varepsilon_0 \varepsilon''} = \frac{1}{\omega \varepsilon_0 \varepsilon' \tan \delta} \tag{4}$$

where $\omega = 2\pi f$ is the angular frequency and ε_o denotes the permittivity in vacuum. The grain and the grain boundaries of ferrite composites have influence on the resistivity of the materials. According to the Koop's theorem, the ferrite composites behave as a multilayer capacitor. With the increase of frequency, the motion of the outermost electrons increases as well as capacitance increases. This increase in capacitance causes on the increase in the electrical conductivity which consequences on the decrease in electrical resistivity [25-26]. In this work, the maximum value of resistivity can be seen for x=0.08 and minimum for x= 0.00 at low temperature. With the increase on frequency, the value of resistivity decreases and reaches at a constant value at high frequency range.

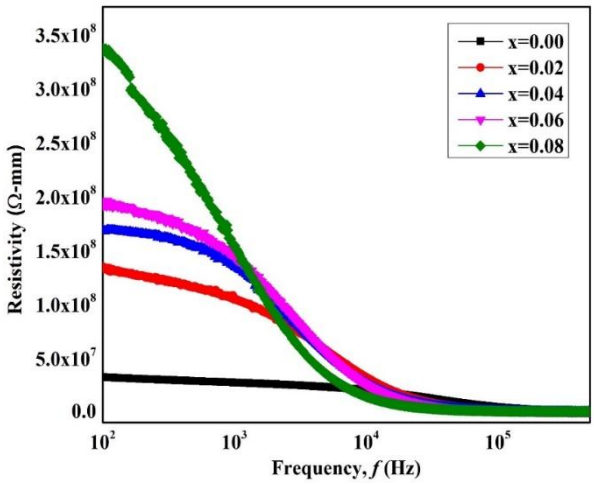

Fig. 5. Variation of the frequency dependent resistivity of $Cu_{0.15}Zn_{0.85}La_xFe_{2-x}O_4$, [x = 0.00, 0.02, 0.04, 0.06 and 0.08].

4. Conclusion

The polycrystalline $Cu_{0.15}Zn_{0.85}La_xFe_{2-x}O_4$ [x = 0.00, 0.02, 0.04, 0.06 and 0.08] were synthesized properly following solid state reaction method and then sintered at 1150 °C for 6 h. The XRD patterns ensure the formation of fcc type spinel cubic structure with secondary peak for x = 0.04 - 0.08. The SEM patterns for all the specimens provide the information that the sample size for all the elements are within 500-1600 nm where the sample size decreases with the increase of La content. The M-H curves for all the samples ensuring the ferromagnetic phenomenon of all the specimens. With the increase of La content, there is an increasing phenomenon of coercivity (H_c) and remanent magnetization (M_r) while saturation magnetization (M_s) decreases. The frequency dependent resistivity delineates the decreasing trend with the increase of applied frequency and obtains constant values at a certain high frequency region.

Acknowledgements

Authors wishing to acknowledge the Solid State Physics laboratory, Department of Physics, Khulna University of Engineering & Technology with deepest sense of gratitude. Also the contribution of Materials Science Division, Bangladesh Atomic Energy Centre, Dhaka is also acknowledged.

References

1. T. Nakamura, J. Magn. Magn. Mater. **168**, 285 (1997). https://doi.org/10.1016/S0304-8853(96)00709-3
2. S. Akhter, D. P. Paul, M. A. Hakim, D. K. Saha, H. N. Das, A. Parveen, and B. Anjuman, Mater. Res. **21**, 1 (2013). https://doi.org/10.1590/1980-5373-mr-2017-0655
3. L. B. Tahar, M. Artus, S. Ammar, L. S. Smiri, F. Herbst, M. -J. Vaulay, V. Richard, J. -M. Grenèche, F. Villain, and F. Fiévet, J. Magn. Magn. Mater. **320**, 3242 (2008). https://doi.org/10.1016/j.jmmm.2008.06.031
4. L. Zhao, H. Yang, X. Zhao, L. Yu, Y. Cui, and S. Feng, Mat. Lett. **60**, 1 (2006). https://doi.org/10.1016/j.matlet.2005.07.017
5. A. A. Sattar, A. H. Wafik, K. M. El-Shokrofy, and M. M. El-Tabby, Physica Status Solidi. (a), **171**, 563 (1999). https://doi.org/10.1002/(SICI)1521-396X(199902)171:2<563::AID-PSSA563>3.0.CO;2-K
6. E. Ateia, M. A. Ahmed, and A. K. El-Aziz, J. Magn. Magn. Mater. **311**, 545 (2007). https://doi.org/10.1016/j.jmmm.2006.08.014
7. M. A. Ahmed, N. N. Okasha, and M. M. El-Sayed, Ceramics Int. **33**, 49 (2007). https://doi.org/10.1016/j.ceramint.2005.07.014
8. C. Nayek, A. Tamilselvan, C. Thirmal, P. Murugavel, and S. Balakumar, J. Appl. Phys. **115**, 073902 (2014). https://doi.org/10.1063/1.4865958
9. K. Nahar, P. Roy, M. A. Hossain, S. D. Nath, N. N. I. Khan, and S. S. Sikder, J. Eng. Sci. **10**, 79 (2019).
10. K. M. Batoo and M. S. Ansari, Nanoscale Res. Lett. **7**, 1 (2012). https://doi.org/10.1186/1556-276X-7-112
11. S. K. Shil, R. C. Sinha, M. A. Hakim, and S. S. Sikder, J. Eng. Sci. **04**, 119 (2013). https://www2.kuet.ac.bd/JES/images/files/PDF_Final_V4_N_1/12_JES_June_2013.pdf

12. M. Vucinic-Vasic, E. S. Bozin, L. Bessais, G. Stojanovic, U. Kozmidis-Luburic, M. Abeykoon, B. Jancar, A. Meden, A. Kremenovic, and B. Antic, J. Phys. Chem. C **117**, 12358 (2013). https://doi.org/10.1021/jp403459t
13. S. Yasmin, S. Choudhury, M. A. Hakim, A. H. Bhuiyan, and M. J. Rahman, J. Ceram. Process. Res. **12**, 387 (2011).
14. A. Anwar, M. A. Basith, and S. Choudhury, Mat. Res. Bull. **111**, 93 (2019). https://doi.org/10.1016/j.materresbull.2018.11.003
15. M. Mustafa, M. J. Rahman, and S. Choudhury, Sci. Eng. Compos. Mater. **26**, 62 (2019). https://doi.org/10.1515/secm-2017-0177
16. M. A. Ali, M. N. I. Khan, F-.U-. Z-. Choudhury, S. Akhter, and M. M. Uddin, J. Sci. Res. **7**, 65 (2015). https://doi.org/10.3329/jsr.v7i3.23358
17. P. K. Mondal, M. A. Hossain, M. N. I. Khan, and S. S. Sikder, Int. J. Phys. Sci. **14**, 21 (2019). https://doi.org/10.5897/IJPS2018.4746
18. Z. Peng, X. Fu, H. Ge, Z. Fu, C. Wang, L. Qi, and H. Miao, J. Magn. Magn. Mater. **323**, 2513 (2011). https://doi.org/10.1016/j.jmmm.2011.05.033
19. N. Rezlescu, E. Rezlescu, C. Pasnicu, and M. L. Craus, J. Phys.: Condensed Matter **6**, 5707 (1994). https://doi.org/10.1088/0953-8984/6/29/013
20. M. N. Akhtar and M. A. Khan, J. Magn. Magn. Mater. **460**, 268 (2018). https://doi.org/10.1016/j.jmmm.2018.03.069
21. M. N. Akhtar, M. Yousaf, S. N. Khan, M. S. Nazir, M. Ahmad, and M. A. Khan, Ceram. Int. **43**, 17032 (2017). https://doi.org/10.1016/j.ceramint.2017.09.115
22. M. F. Din, I. Ahmad, M. Ahmad, M. T. Farid, M. A. Iqbal, G. Murtaza, M. N. Akhtar, I. Shakir, M. F. Warsi, and M. A. Khan, J. Alloys Compd. **584**, 646 (2014). https://doi.org/10.1016/j.jallcom.2013.09.043
23. A. I. Ali, M. A. Ahmed, N. Okasha, M. Hammam, and J. Y. Son., J. Mat. Res. Technol. **2**, 356 (2013). https://doi.org/10.1016/j.jmrt.2013.09.001
24. M. A. Ahmed, E. Ateia, and S. I. El-Dek, Mat. Lett. **57**, 4256 (2003). https://doi.org/10.1016/S0167-577X(03)00300-8
25. M. F. Al-Hilli, Iraqi J. Phys. **9**, 6 (2011). https://www.iasj.net/iasj?func=fulltext&aId=66474
26. S. A. Mazen, Mat. Chem. Phys. **62**, 139 (2000). https://doi.org/10.1016/S0254-0584(99)00158-3